ELSEVIER

Thermochimica Acta 269/270 (1995) 117–132

thermochimica acta

Microstructural characterisation of Ni, Co and Ni–Co fine powders for physical sensors ☆

A. Bianco, * G. Gusmano, R. Montanari, [a] G. Montesperelli, E. Traversa

Dipartimento di Scienze e Tecnologie Chimiche [a] Dipartimento di Ingegneria Meccanica, Universita' di Roma Tor Vergata, Via della Ricerca Scientifica, 00133 Roma, Italy

Received 2 November 1994; accepted 2 May 1995

Abstract

Thick-film magnetoresistive sensors based on Ni and Co fine powders have shown promising results. In order to improve their performance Ni, Co and Ni–Co powders were prepared by the polyol process. The metallic powders were characterised by simultaneous thermogravimetric and differential thermal analysis (TGA–DTA), X-ray diffraction analysis (XRD) and scanning electron microscopy (SEM).

Keywords: Co fine powders; Microstructure; Ni fine powders; Ni–Co fine powders; SEM; TGA–DTA; XRD

1. Introduction

Fine Ni, Co and Ni–Co alloy powders are required for developing magnetoresistive sensors in thick-film form [1–4]. These sensors can detect and measure physical quantities such as distance, linear and angular position and rotation speed [5]. Thick films obtained by firing in N_2 pastes based on commercial Ni and Co fine powders (Ni/Co atomic ration, a.r., 70/30) have shown good results [6]. It is expected, however, that devices based on finer Ni and Co powders or on Ni–Co alloy powders should show larger magnetoresistance anisotropy and lower thermal coefficient of resistance [7].

It has been reported that the reduction of M(II) and M(I) inorganic compounds in polyols gives good yields of micronic and submicronic metallic powders, the polyol

* Corresponding author.

☆ Presented at the 6th European Symposium on Thermal Analysis and Calorimetry, Grado, Italy, 11–16 September 1994.

SSDI 0040-6031(95)02531-6

acting both as reaction medium and reducing agent [8]. The first step of the reaction is the dissolution of the precursors, then the reduction in the liquid phase occurs. Finally, the nucleation and growth of the metallic phase take place [9].

In previous papers [10–12] the authors have reported the preparation of Ni, Co and Ni–Co powders starting from different precursors in various polyols. This paper mainly deals with the microstructural characterisation of the metallic powders obtianed by the use of various techniques in combination.

Information on the chemical composition (presence of unreacted precursors or by-products) and the microstructure of the Ni, Co and Ni–Co powders was first obtained by DTA–TGA. The characterisation was completed by XRD analysis and SEM observations.

2. Experimental

2.1. Materials

Ni, Co and Ni–Co alloy powders were prepared as described below. The preparation of the M(II) precursors has been reported elsewhere [10–12]. The commercial chemicals were Aldrich (Reagent Purity Grade).

Ni powders

30 mmol of freshly prepared Ni(II) bis-acetylacetonate ($Ni(acac)_2$) were added to 300 ml of 3,6-dioxaoctane-1,8-diol (triethyleneglycol, TEG) (b.p. 285°C).

Co powders

15 mmol of Co(II) bis-acetylacetonate ($Co(acac)_2$), commercial (a) or freshly prepared (b), were added to 30 ml of 1,2-ethanediol (ethylene glycol, EG) (b.p. 196–198°C).

Ni–Co powders

(a) 30 mmol of commercial Ni(II) acetate tetrahydrate ($Ni(OAc)_2 \cdot 4H_2O$) and 10 mmol of commercial Co(II) acetate tetrahydrate ($Co(OAc)_2 \cdot 4H_2O$) were added to 100 ml of EG.

(b) 30 mmol of commercial Ni(II) acetate tetrahydrate ($Ni(OAc)_2 \cdot 4H_2O$) and 10 mmol of commercial Co(II) acetate tetrahydrate ($Co(OAc)_2 \cdot 4H_2O$) were added to 100 ml of 2,2′-oxydiethanol (diethylenglycol, DEG) (b.p. 285°C).

(c) 48 mmol of freshly prepared Ni(II) hydroxide ($Ni(OH)_2$) and 15 mmol of Co(II) hydroxide ($Co(OH)_2$) were added to 100 ml of EG.

The mixtures were refluxed in air under magnetic stirring. In the case of $Ni(acac)_2$ the reactions were performed by refluxing the mixtures in air (a) and in water (b).

The products were washed with acetone and dried at room temperature. All the metallic powders were obtained in good yields.

2.2. Measurements

The precursors and the powders obtained were characterised by the following techniques:

X-ray diffraction analysis (XRD) (Philips mod. PW 1729)

The XRD patterns were recorded using Zr-filtered MoKα radiation ($\lambda = 0.071$ nm) in the 2θ range from 5° to 65°. Precision line profiles were obtained by step scanning with 2θ angular intervals of 0.005° and counting times of 20 s for each step. Better resolved XRD spectra were obtained using V-filtered CrKα radiation ($\lambda = 0.229$ nm).

Simultaneous thermogravimetric and differential thermal analysis (TGA–DTA) (Netzsch mod. STA 409)

The analyses were performed in static air, heating rate 5°C min^{-1}, sample weight about 25 mg, reference sample alumina.

Quantitative analysis

The Ni/Co atomic ratio (a.r.) was determined following a volumetric procedure described in the literature [13]. Scanning electron microscopy (SEM) was performed with a Leica (Cambridge) mod. Stereoscan 360.

3. Results and discussion

3.1. Ni powders

In Fig. 1 is reported the thermal behaviour of Ni powders (a) and (b). Thermal analysis of Ni powder (a) showed, on the DTA curve in the range 400–700°C, a small exothermic signal at 400°C and a rather broad exothermic peak with its minimum at 570°C. A 27% weight-gain was detected on the TG curve.

The observed transformation was attributed to the oxidation of Ni to Ni(II) oxide (NiO), as confirmed by XRD analysis performed on the product obtained after the TGA–DTA measurements [14], and by literature data [15].

The DTA curve of Ni powder (b) showed a sharp exothermic peak with its minimum at 380°C and a low-intensity exothermic bump with its minimum at 425°C. On the TGA curve was recorded in the range 300–380°C a 5% weight-gain followed by a weight loss of 2%. In the range 380–470°C a 15% weight-gain was found.

The effect around 400°C could be attributed to the superimposition of the oxidation of the metal powder and the decomposition of traces of unreacted organometallic precursor. The second transformation was associated with the oxidation in air of the Ni powder.

It should be taken into consideration that the oxidation in air of the metallic powders could lead to the formation of mixed oxide–nitride phases. However the investigated techniques did not allow us to discriminate between the oxides and mixed oxide–nitride phases.

The XRD patterns of Ni powders (a) and (b) are reported in Fig. 2. Ni powder (a), obtained by refluxing the mixture in air, showed only the reflections of the face cubic centred (f.c.c.) Ni lattice [16]. In the case of Ni powder (b), obtained by refluxing the mixture with water, peaks of nickel carbide (Ni_3C) were also detected [17]. The

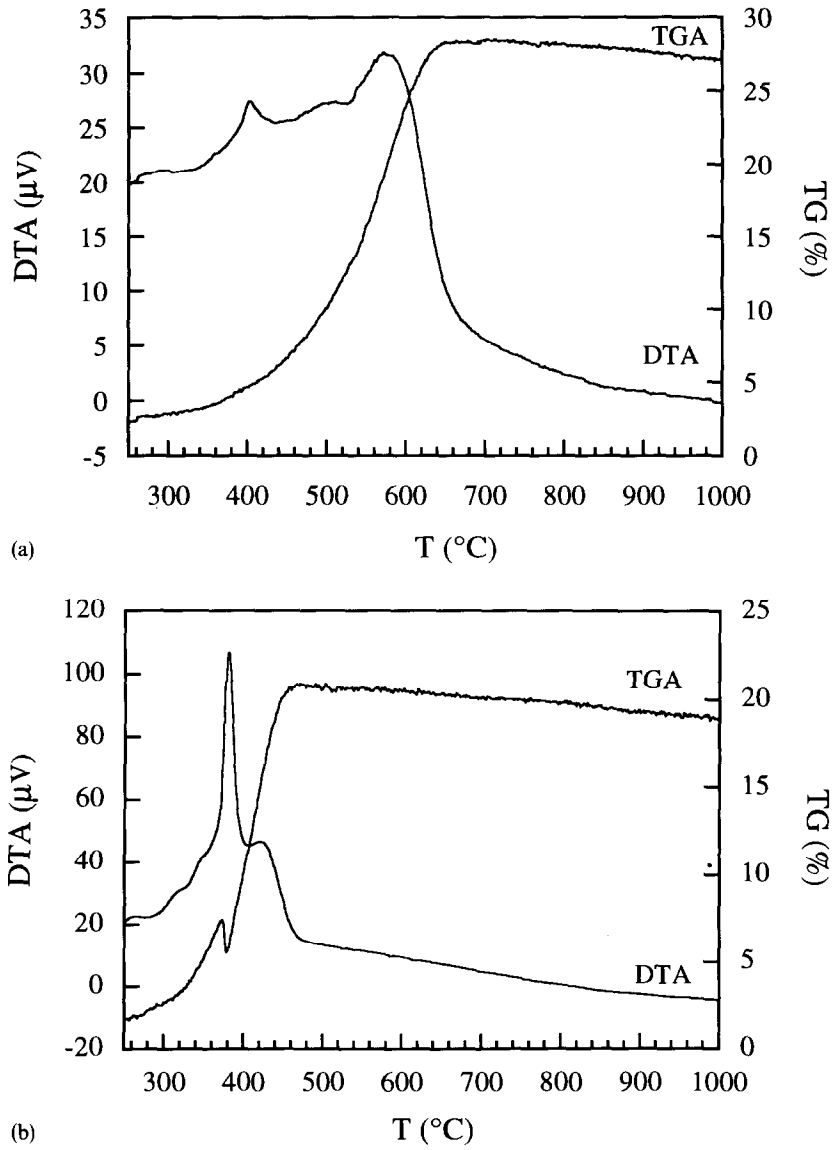

Fig. 1. TGA–DTA patterns of Ni powder (a) (1a) and Ni powder (b) (1b).

presence of Ni_3C as a by-product in Ni powders obtained in TEG has already been observed by other authors [18].

By comparing the two thermal analysis patterns reported in Figs. 1a and 1b, it was observed that the oxidation of Ni powder (b) occurs in a lower and narrower temperature range than that of Ni powder (a).

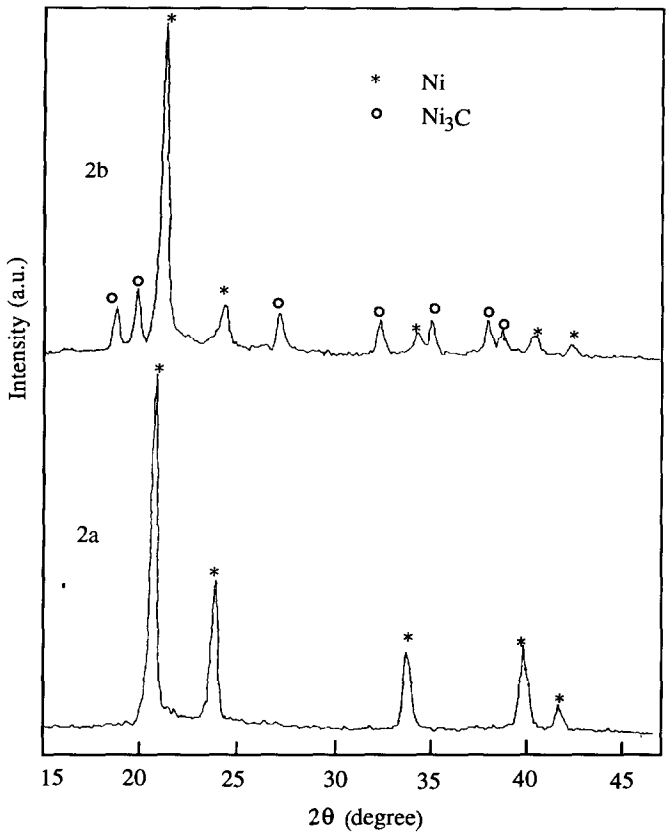

Fig. 2. XRD (MoKα) profiles of Ni powder (a) (2a) and Ni powder (b) (2b).

Fig. 3 shows the SEM micrographs of Ni powders (a) and (b). The particle diameters of Ni powder (a) ranged around 700 nm, while for Ni powder (b) an average particle size of 150 nm was observed. Therefore, the different thermal behaviour may be due to the lower mean particle size of Ni powder (d) compared to Ni powder (a).

Thus, products with different chemical purities and microstructures can be obtained by reducing the same precursor in the same polyol, depending on the experimental conditions.

3.2. *Co powders*

XRD patterns of Co powders showed a highly distorted hexagonal closed packed (h.c.p.) lattice (Fig. 4). In Table 1 the 2θ experimental positions obtained with precision measurements are compared with those calculated for MoKα radiation using data reported in literature [19]. The peak profiles were broadened and the d_{hkl} values were smaller than those reported in the literature [19]. Due to their preparation, the

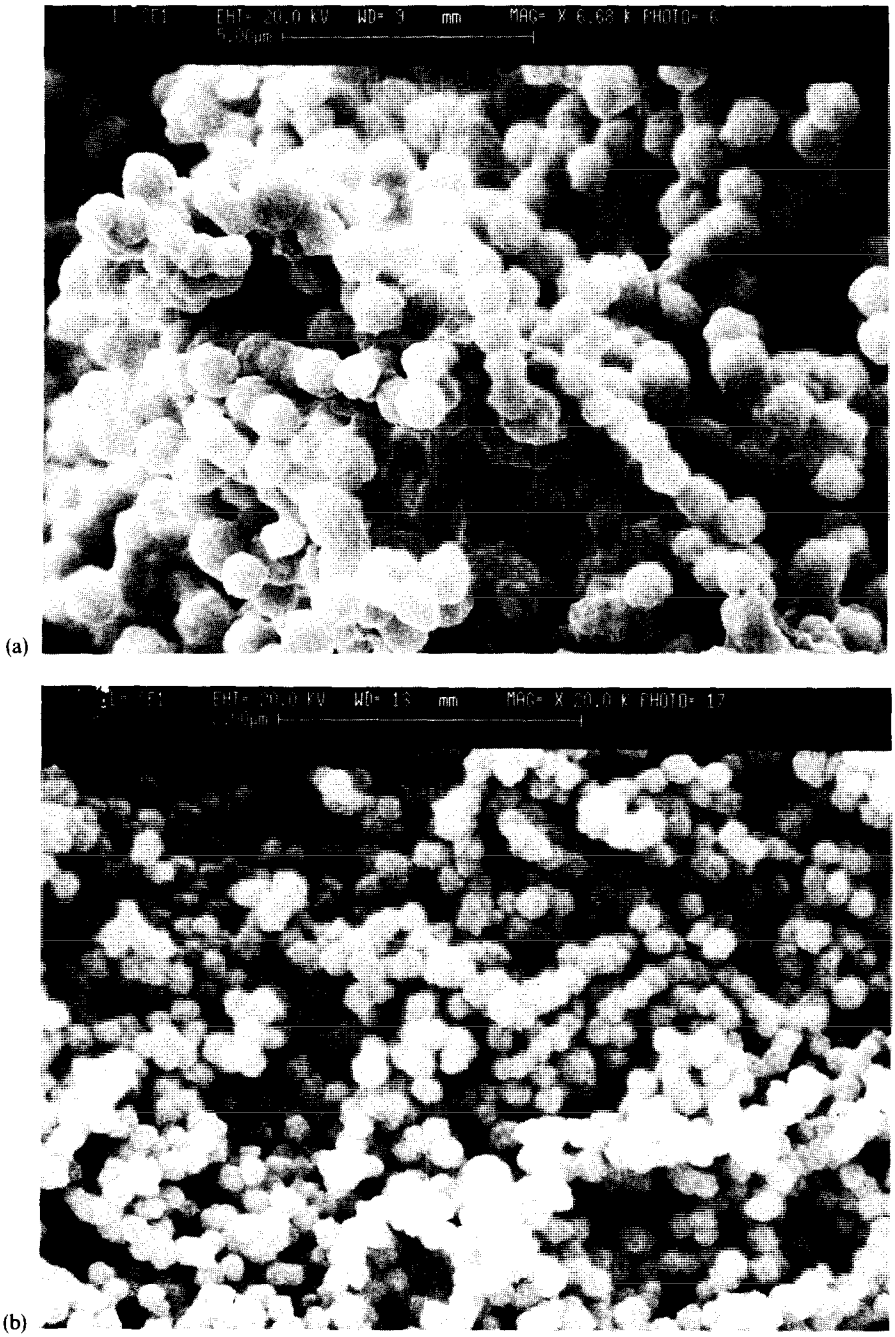

(a)

(b)

Fig. 3. SEM micrographs of Ni powder (a) (3a) and Ni powder (b) (3b).

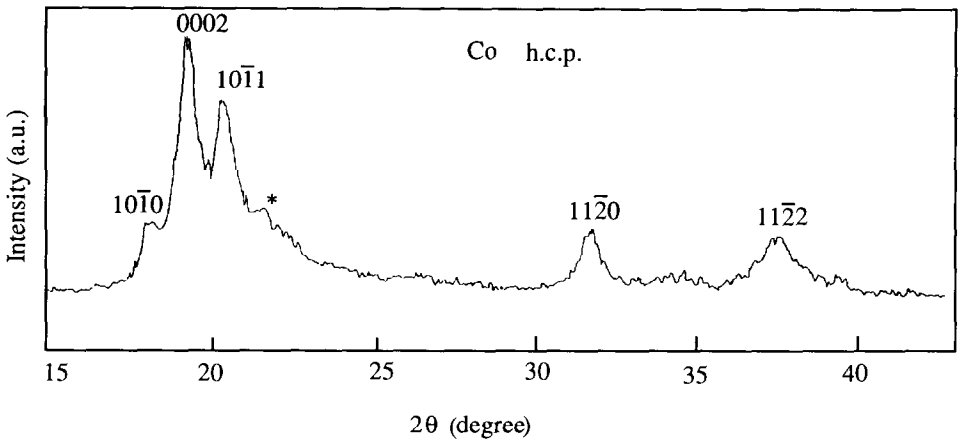

Fig. 4. XRD (MoKα) profile of Co powder (a).

Table 1
Comparison between 2θ(/°) positions and d(/nm) values obtained by XRD (MoKα) precision measurements (exp.) of Co (a) powder and those calculated (cal.) for Co h.c.p. using literature data [19].

(hkil)	10$\bar{1}$0	0002	10$\bar{1}$1
2θ, exp.	19.19	20.39	21.59
$d \times 10^{-1}$, exp.	2.13	2.00	1.89
2θ, cal.	18.87	20.21	21.42
$d \times 10^{-1}$, cal.	2.16	2.02	1.91

powders were considered dislocation-free, and thus the observed peak broadening was due to the small size of the crystallites which diffract coherently. This effect was more evident in the case of Co powder (b), obtained from synthesized $Co(acac)_2$. The low intensity peak centered at 22.1° (2θ) indicated with the symbol (*) in Fig. 4 does not correspond to an h.c.p. reflection. In order to achieve better resolution the XRD pattern was recorded using CrKα radiation but also in this case the peak appears very broadened. Therefore, it was supposed that stacking faults in high density were present in the h.c.p. lattice, giving raise to zones with f.c.c. packing inside the h.c.p. grains. An analogous peak was observed by Cardellini and Mazzone in pure h.c.p. Co powders ball-milled for 20 h; this was attributed to the (200) reflection of Co f.c.c. [20].

Thermal analysis performed on Co powder (a) (Fig. 5a) showed, on the DTA curve, a broad exothermic peak with its minimum at 410°C, two exothermic peaks with their minima at 680°C and 760°C, and finally a sharp endothermic peak with its maximum at 930°C. The TGA patterns showed three distinct steps. In the range 360–670°C, a 13% weight-gain was found, a 19% weight-gain was recorded in the range 670–880°C, and finally in the range 900–950°C a 9% weight-loss (with respect to Co) was detected.

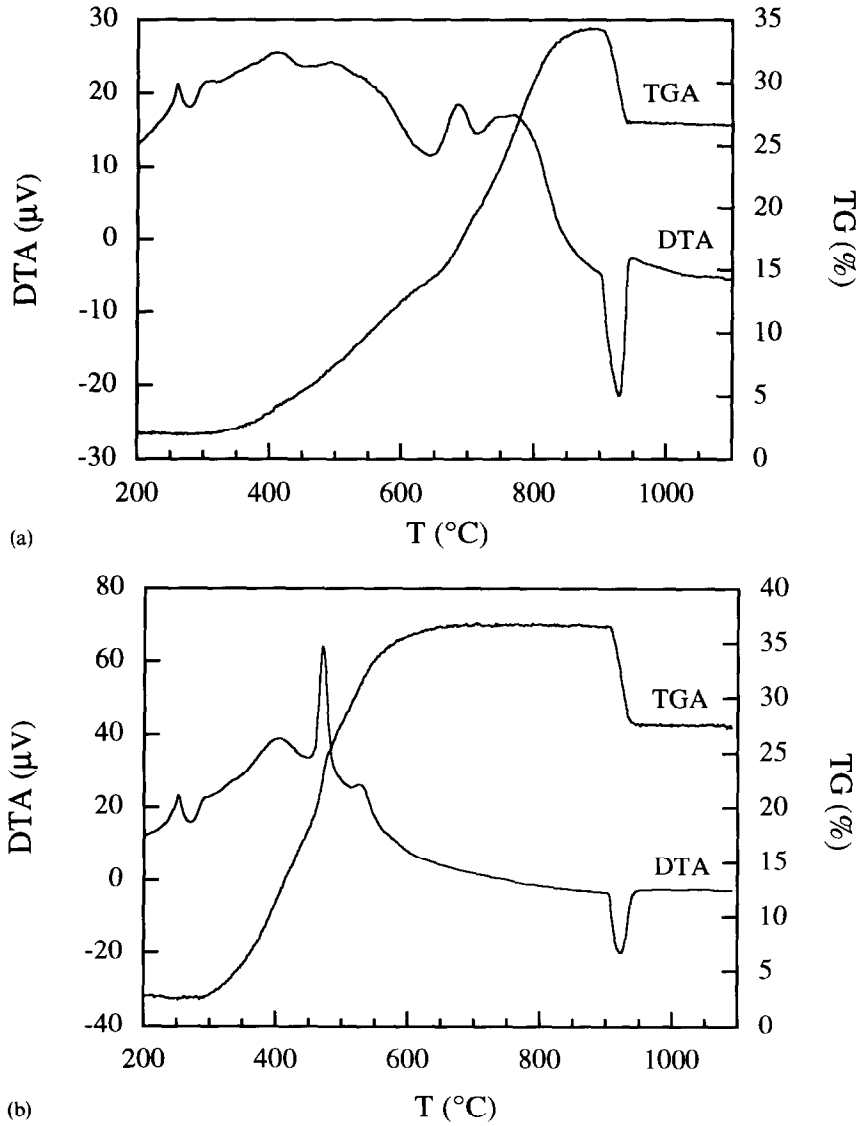

Fig. 5. TGA–DTA patterns of Co powder (a) (5a) and Co powder (b) (5b).

Fig. 5b shows the thermal behaviour of the Co powder (b). The DTA curve showed two exothermic peaks with their minima at 400°C (broad) and 470°C (sharp), a shoulder at 530°C, and finally a sharp endothermic peak with its maximum at 920°C. Both DTA patterns showed a small exothermic peak at 260°C.

On the TGA curve a sample weight-gain of 34% was recorded in the range 300–600°C, and a 9% weight-loss (with respect to Co) was recorded in the temperature range of the last DTA peak.

The TGA curve of Co powder (a) showed a slope change occurring around 670°C, while a linear trend was observed in the case of Co powder (b) up to 600°C.

In order to explain this different behaviour, Co powders (a) and (b) were both heated to 670°C (heating rate 5°C min^{-1}). The XRD patterns are reported in Figs. 6 and 7.

The XRD spectrum of sample (a) (Fig. 6a) showed Co(II, III) oxide (Co_3O_4) reflections [21]; some other lines of minor intensity were also detected. To identify the other phases present in the mixture XRD measurements were performed by using CrKα radiation which gives better resolution (Fig. 7).

The peaks at 55.7 and at 56.3° (2θ) in Fig. 7, which correspond to CoO (111) [22] and Co_3O_4 (311) respectively, appear in Fig. 6 as a single line. Fig. 7 shows that the line at 20.2° (2θ) in Fig. 6 is also due to the overlapping of two reflections corresponding to Co f.c.c. (111) [23] and Co_3O_4 (400). Therefore the two main reflections (111) and (200) of Co f.c.c. confirm that besides Co_3O_4 and CoO Co f.c.c. is also present in sample (a) heated to 670°C. No reflections related to the Co h.c.p. phase were detected.

As shown in Fig. 6b, the XRD pattern of Co powder (b) heated to 670°C did not show any signals related to Co f.c.c. or to Co h.c.p.. Reflections of CoO were found for this sample also. These results were confirmed by CrKα radiation XRD spectra.

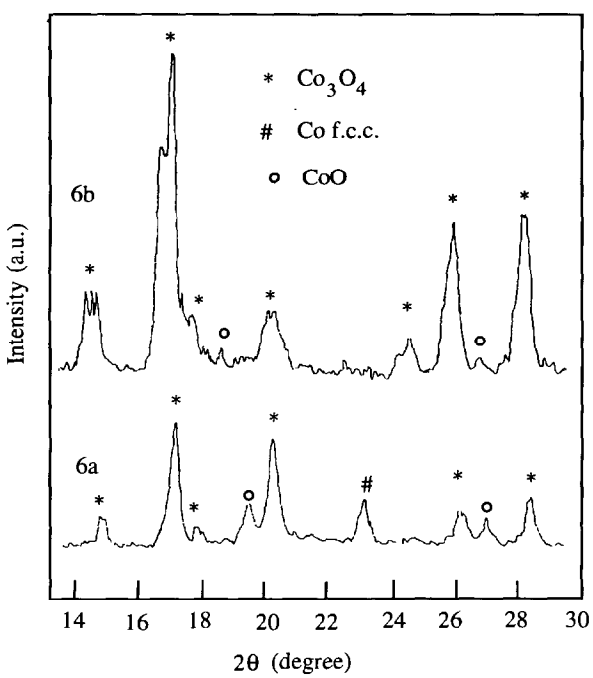

Fig. 6. XRD (MoKα) profiles of Co powders (a) (6a) and Co powders (b) (6b).

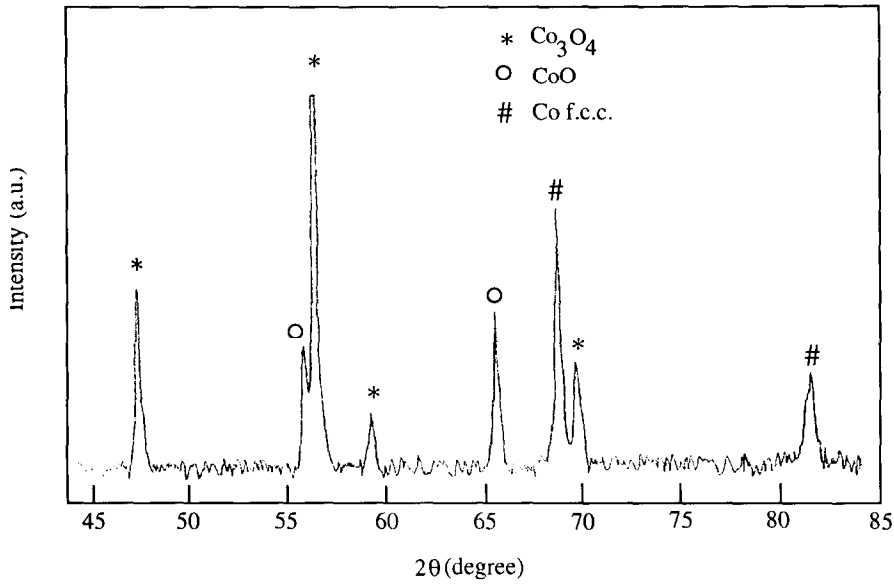

Fig. 7. XRD (CrKα) profiles of Co powders (a) after heating to 670°C.

Both Co powders (a) and (b) heated to 1200°C showed mostly CoO peaks [22] (Fig. 8). These results are in agreement with literature data [15] and with the thermal behaviour observed for the commercial Co powder (Aldrich).

It was supposed that the different oxidation rates of Co powders were due to the different microstructural features.

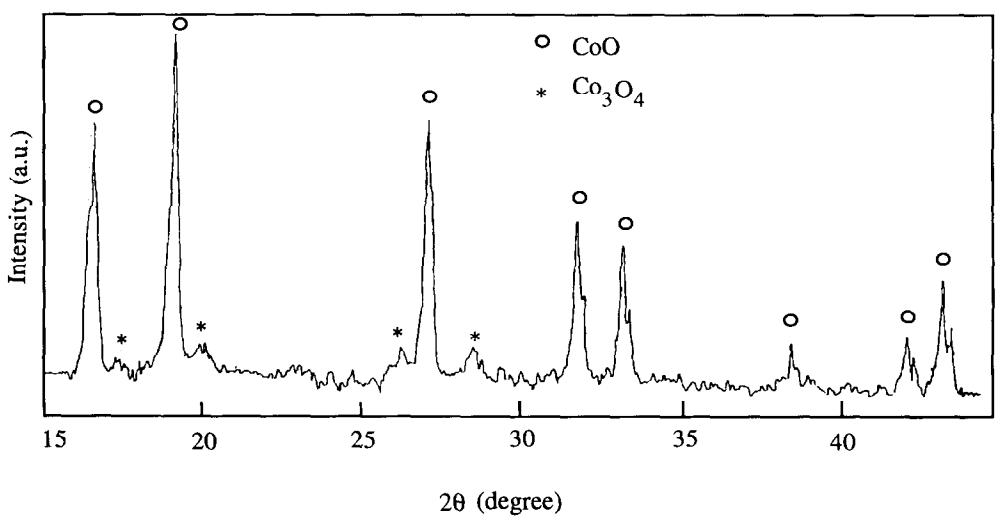

Fig. 8. XRD (MoKα) profile of Co powder (a) heated to 1200°C.

SEM micrographs of Co powders shown in Fig. 9 confirm this hypothesis, since Co powder (a) was more heavily agglomerated than Co powder (b). These results explain the slower oxidation rate of the former observed by means of the thermal analysis.

3.3. *Ni–Co alloy powders*

The thermal behaviour of the Ni–Co alloy powders was characterised on the DTA curve by a small exothermic peak at 280°C followed by a sharp exothermic peak in the range 300–700°C. On the TGA curve a sample weight-gain of 27% was observed. Fig. 10 shows the TGA–DTA pattern of Ni–Co powder (c) (Ni/Co a.r. 70/30). The experimental results suggested that the oxidation of the Ni–Co alloy to (Ni(II), Co(II)) oxide ((Ni, Co)O) occurred.

The XRD patterns of the Ni–Co alloy showed only the reflections of a Ni-like f.c.c. pattern, as reported in previous papers [10–12]. No peaks related to the precursors, to by-products or to the single metals were detected.

The XRD spectrum of Ni–Co alloy powders heated to 1200°C showed an NiO-like lattice pattern only, and no reflections related to cobalt or nickel oxides were found (Fig. 11).

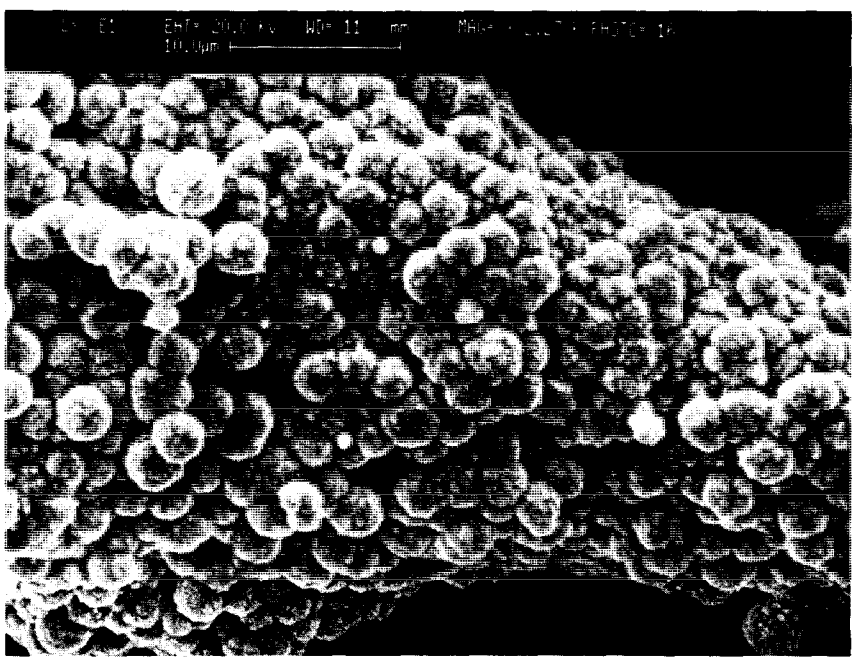

(a)

Fig. 9. SEM micrographs of Co powder (a) (9a) and Co powder (b) (9b).

(b)

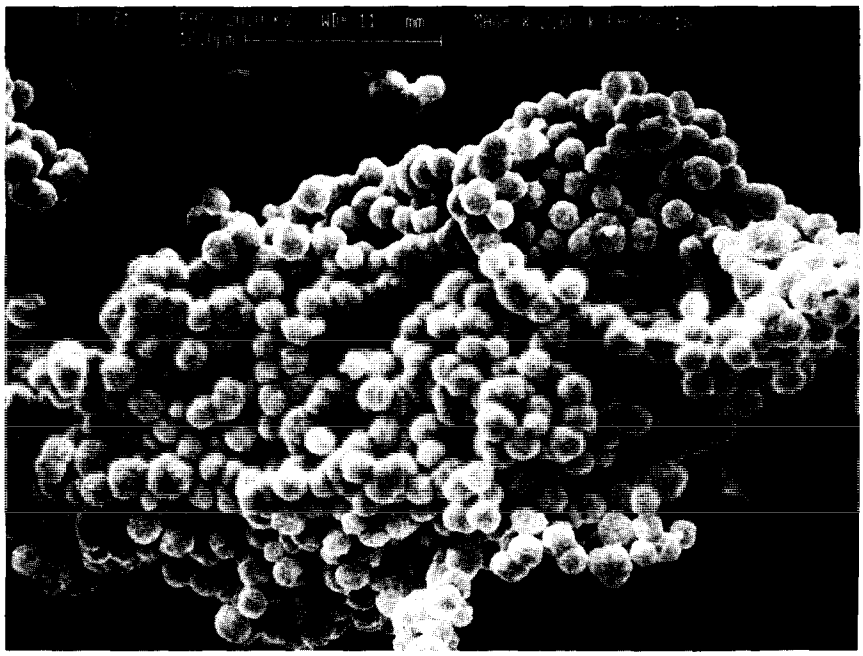

Fig. 9. (*Continued*)

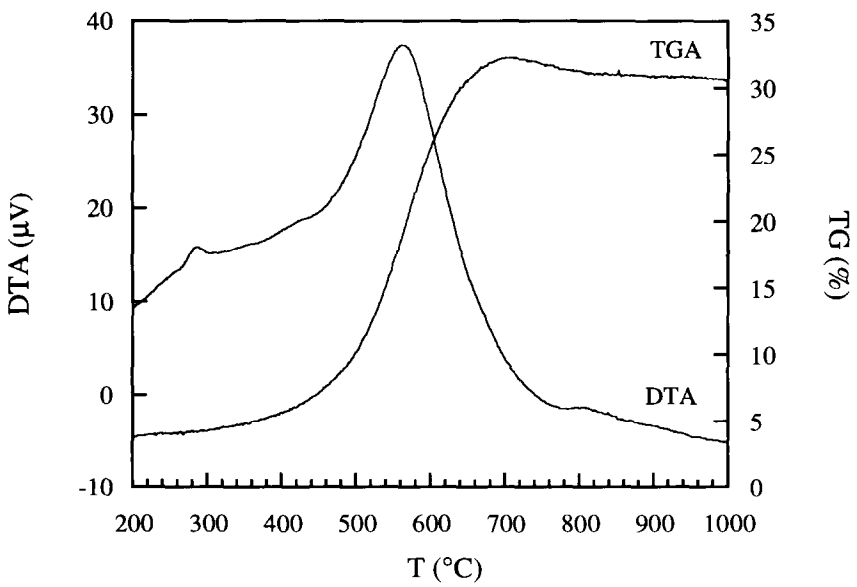

Fig. 10. TGA–DTA patterns of Ni–Co powder (c).

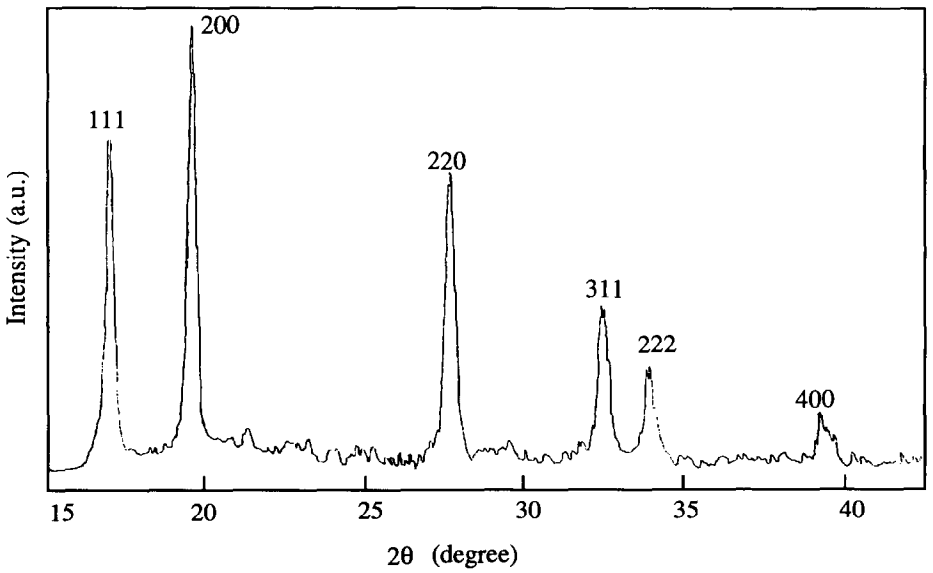

Fig. 11. XRD (MoKα) profile of Ni–Co powders heated to 1200°C.

The DTA patterns of Ni–Co alloy powders are compared in Fig. 12. The DTA curve of Ni–Co (a) (Ni/Co a.r. 90/10) showed an exothermic peak in the range 400–700°C. In the case of Ni–Co (b) (Ni/Co a.r. 70/30) the peak is split and shifted in the range 300–600°C.

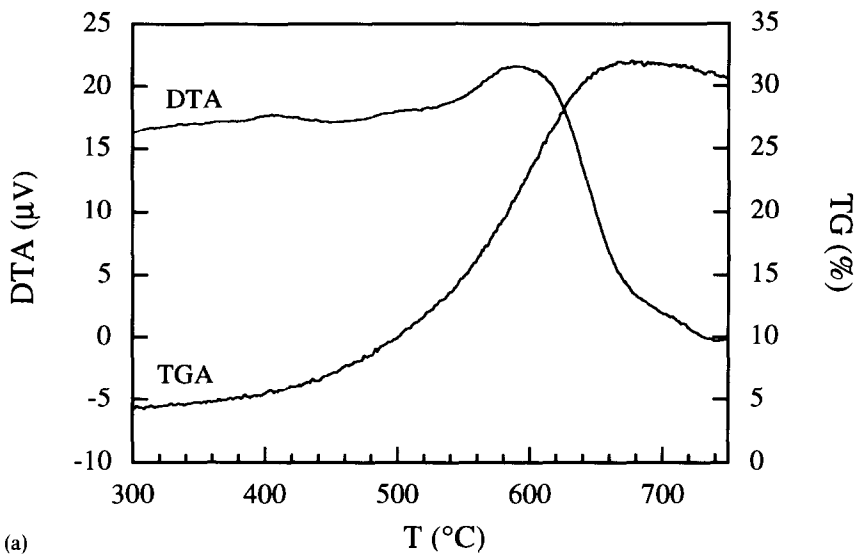

Fig. 12. TGA–DTA patterns of Ni–Co powders (a) (12a) and (b) (12b).

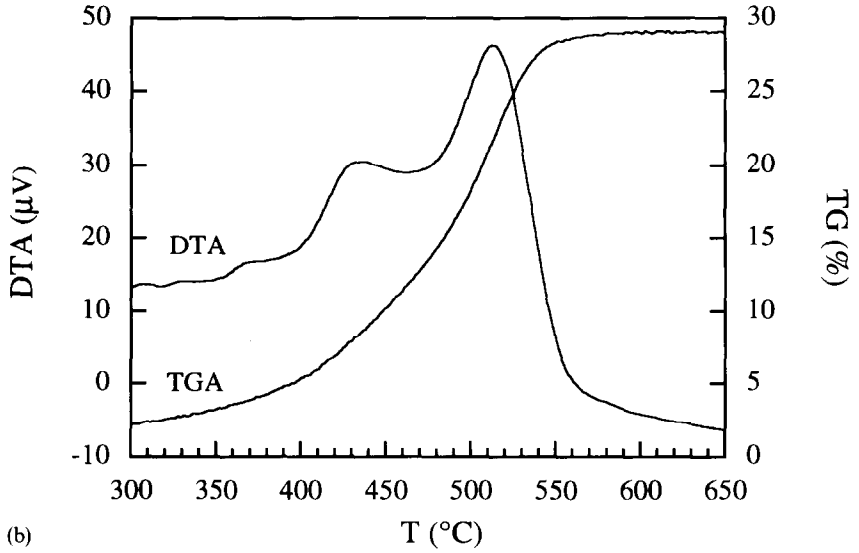

(b)

Fig. 12. (*Continued*)

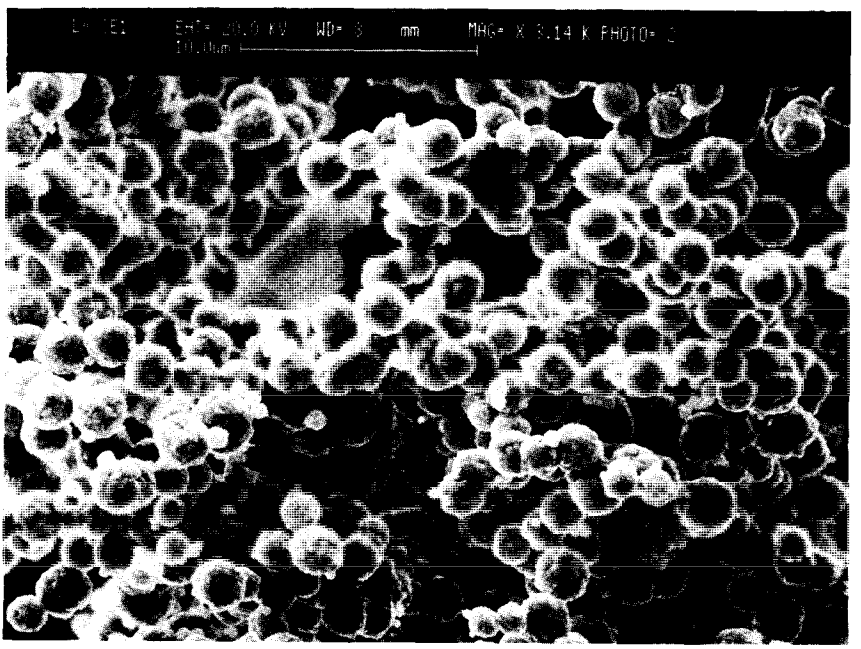

(a)

Fig. 13. SEM micrographs of Ni–Co powder (a) (13a) and Ni–Co powder (b) (13b).

(b)

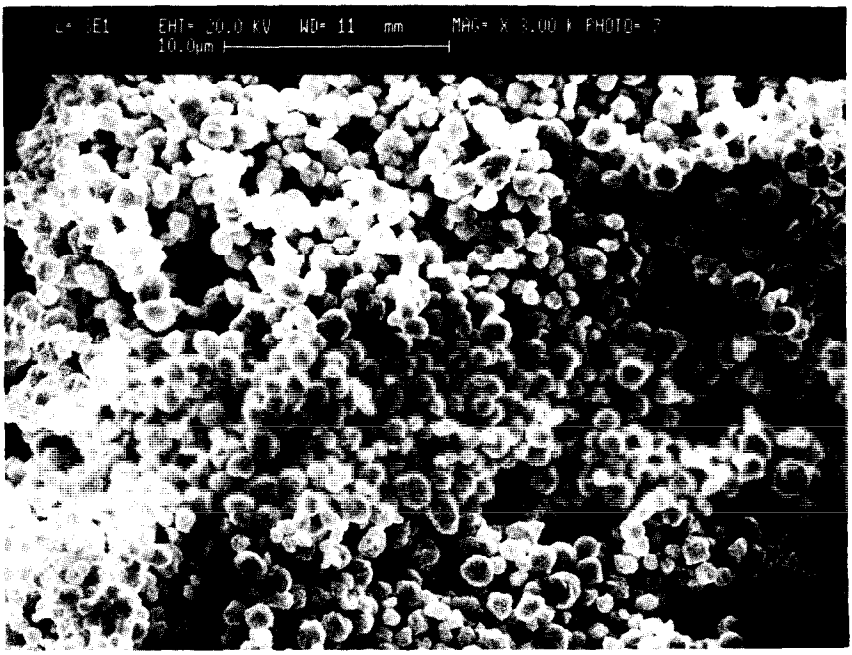

Fig. 13. (*Continued*)

Once more the different thermal behaviour was attributed to the different powders' microstructures. This was explained in terms of more homogeneous and less agglomerated particles of Ni–Co (b) powder than Ni–Co (a) powder. These results were confirmed by SEM, as shown in Fig. 13.

Thus, the microstructure of the Ni–Co alloy powders depends strictly on the polyol used as reaction medium, as observed by other authors in the case of single metals [24].

As already observed in the case of Ni powders, the techniques used did not furnish experimental evidence of the formation of mixed oxide–nitride compounds.

4. Conclusions

Ni, Co and Ni–Co powders were obtained by reduction of M(I) and M(II) inorganic precursors in polyols. The products were first characterised by thermal analysis to check the chemical purity and to detect and identify unreacted precursors or by-products. By means of thermal analysis, preliminary microstructural information was obtained and subsequently confirmed by XRD analysis and SEM observations. The chemical purity, the atomic composition and the microstructure of the metallic powders were greatly affected by the precursors, by the polyol and by the experimental conditions under which the reactions occurred.

Acknowledgement

This work was partially supported by the Italian National Research Council (C.N.R.), under the auspices of the Targeted Project "Special Materials for Advanced Technologies".

References

[1] T.R. McGuire and R.I. Potter, IEEE Transactions on Magnetics, 11 (1975) 1018.
[2] B. Morten, M. Prudenziati, F. Sirotti, G. De Cicco, A. Alberigi-Quaranta and L. Olumekor, J. Mater. Sci.: Materials in Electronics, 1 (1990) 118.
[3] F. Sirotti, M. Prudenziati, T. Manfredini, B. Giardullo and W. Anzolin, J. Mater. Sci., 25 (1990) 4688.
[4] M. Prudenziati and B. Morten, Microelectron. J., 23 (1992) 133.
[5] B. Morten, G. De Cicco, M. Prudenziati, A. Masonero and G. Mihai, Proc. VIII Eurosensors, Toulouse, France, September 1994 (in press).
[6] L. Obici, M. Phys. Thesis, University of Modena, Italy, 1992.
[7] U. Dibbern, Sensors and Actuators, 10 (1986) 127.
[8] B. Blin, F. Fievet, D. Beaupere and M. Figlarz, New J. Chem., 13 (1989) 67.
[9] F. Fievet, J.P. Lagier, B. Blin, B. Beaudoin and M. Figlarz, Solid-State Ionic, 32/33 (1989) 198.
[10] A. Bianco, G. Gusmano, R. Montanari, G. Montesperelli and E. Traversa, Mater. Lett., 19 (1994) 263.
[11] A. Bianco, B. Floris, G. Gusmano, R. Montanari, G. Montesperelli and E. Traversa, in P. Vinvenzini (Ed.), New Horizon for Materials, Techna, Faenza, 1995, p. 193.
[12] A. Bianco, Proc. AIMAT 94, Trento, Italy, September 19–21, 1994, Vol. 2, p. 687.
[13] W.F. Harris and T.R.Sweet, Anal. Chem., 26 (1954) 1648.
[14] Powder Diffraction File n. 4-835, JCPDS, 1991.
[15] O. Kubaschewski and B.E. Hopkins, Oxidation of Metals and Alloys, Butterworths, London, 1962.
[16] Powder Diffraction File n. 4-850, JCPDS, 1991.
[17] Powder Diffraction File n. 6-697, JCPDS, 1991.
[18] M. Figlarz, F. Fievet and J.P. Lagier, Patent. Chem. Abstr., 101 (22) 195866.
[19] Powder Diffraction File n. 5-727, JCPDS, 1991.
[20] F. Cardellini and G. Mazzone, Philos. Mag., A67 (1993) 1289.
[21] Powder Diffraction File n. 9-418, JCPDS, 1991.
[22] Powder Diffraction File n. 9-402, JCPDS, 1991.
[23] Powder Diffraction File n. 15-806, JCPDS, 1991.
[24] F. Fievet, J.P. Lagier, B. Beaudoin and M. Figlarz, Reactivity of Solids, Elsevier, Amsterdam, 1985.